Current Ripple Minimisation in Deadbeat Parameter-Free Predictive Control of Synchronous Motor Drives

SILVERIO BOLOGNANI [1] (Fellow, IEEE), **PAOLO GHERARDO CARLET** [1] (Member, IEEE),
FABIO TINAZZI [2] (Member, IEEE), **AND MAURO ZIGLIOTTO** [2] (Senior Member, IEEE)

[1] Department of Industrial Engineering, University of Padova, 35122 Padua, Italy
[2] Department of Management and Engineering, University of Padova, 36100 Vicenza, Italy

ABSTRACT This paper proposes a motor parameter-free predictive current control of synchronous motor drives. In the context of motor parameter-free controls, the distinctive feature proposed in this paper is the use of the discrete space vector modulation technique. The advantages of the proposed architecture are manifold. As a distinctive feature of the proposed control algorithm compared to model-based solutions, is the real-time self-adaptation capability to the installed motor. Two recursive least-square estimators update runtime an accurate non parametric model. Compared to previous parameter-free solutions, the proposed algorithm can achieve a significantly lower current harmonic distortion at the same control frequency, while keeping the switching frequency value at bay. The result is an efficient and smooth torque delivery. The paper gives the necessary design hints and analyses the steady state performance in terms of both current harmonic distortion and switching frequency, taking finite-set model-based and parameter-free schemes as benchmark. This analysis was previously missing in literature for parameter-free schemes. Experimental validation is completed by including dynamic test results.

INDEX TERMS Control of permanent magnet synchronous motor drives (PMSM), model predictive control (MPC), model-free control, data-driven control.

I. INTRODUCTION

The model predictive control (MPC) of the phase currents in a synchronous electric motor is an hot-topic in the scientific literature [1]. The technology advances in the production of new motors, such as interior permanent magnet motors, permanent magnet assisted synchronous reluctance motors and pure synchronous reluctance (SyR) motors expand the application areas of the predictive control paradigm [2].

MPC algorithms can be of the indirect and direct type. Techniques falling into the former group are also know as Continuos Set (CS) MPC [3]–[6]. The CS-MPC effective implementation requires quadratic programming solvers for selecting the optimal voltage vector to be applied. Furthermore, a modulation strategy must be adopted in the CS-MPC, e.g. pulse width modulation (PWM), which adds further complexity and computational burden. The direct MPC techniques are called Finite Set (FS) MPC [7], [8]. The converter bus voltage is not modulated, and the amount of voltage directly applied to the motor windings depends on the inverter swtiches states. The optimal combination of the switches states is selected among a finite set of voltage vectors, called *candidates*, that depends on the power converter topology. In case of a three-phase two-levels inverter, there are eight candidates, including two zero voltage vectors, which correspond to the eight possible switches configurations.

The FS-MPC offers several advantages, such as the modulator removal eases the current regulation scheme. Furthermore, the average switching frequency is reduced with respect to the PWM-based solutions [9]. Thanks to these advantages, FS-MPCs are an effective control method for high power converters [10], where the minimisation of switching losses can lead to an increase of the inverter efficiency.

Finally, the FS-MPC framework is suitable for including additional constraints, e.g. maximum output currents, or to to implement straightforwardly nonlinear cost objectives.

A common issue of the MPCs, both FS and CS, is the need of an accurate model of the plant. The accurate modelling is a challenging task to be accomplished when implementing anisotropic synchronous motors, due to the non-linearities of the flux-current relationships. Advanced identification techniques have been proposed, such as [11], due to the magnetic saturation in anisotropic motors. Alternatively, the control scheme can be integrated with additional online parameter estimation algorithms [12], [13].

As a new paradigm in the scientific research, the motor model can be replaced by an adaptive model which does not require information about the motor parameters. The name *motor parameter-free* was used in [14], which was formerly known as *model-free* in [15]–[17]. A similar approach was used in [18], [19] under the name of MPC based on an *ultra local model*.

The model-free concept has been extended to other power electronics applications, such as a generic auto-regressive with exogenous input model in [20], which is suitable for describing generic voltage source inverter systems. Induction motor drives are considered too, as proposed in [21]. A PWM-based rectifier was considered in [22], including unbalanced and distorted network conditions. Finally, the generality allowed by the model-free approach is further testified by its application to a multilevel inverter in [23]. These methods present all the advantages of online parameter estimation schemes. Many non-linear phenomena, not modelled in the parametric representation, are included since the algorithms do not rely on parametric models. Therefore, a time-consuming and complex identification technique of the motor model can be avoided. Furthermore, an adaptive model can be adopted to any synchronous motor topology, with or without permanent magnets.

One of the main limitations of the algorithm [14] derives from the FS nature of the controller. For instance, the control frequency was kept low due to computational power limitation. The control frequency is often chosen to be equal to the frequency of switches state updating. The cardinality of the voltage vector set is thus limited to the eight base voltage vector, and the problem of finding the optimum solution is reduced. However, if the control frequency is not high enough, the currents harmonic distortion could be significant. Of course, increasing the switches state adaptation frequency, thus the control frequency, results in a higher switching frequency.

In order to improve the current harmonic content, the switches state updating frequency should be increased. However, the control frequency should be decoupled from the switches state updating one to keep the computational effort at bay. This is the underlying concept of the Discrete Space Vector Modulation (DSVM) introduced in [24]. According to the DSVM, the control period is divided in a discrete number of sub-periods. Any of the eight voltage vector candidates

can be applied in each sub-period. According to a benchmark DSVM, the voltage vectors synthesised by the modulation are mapped in look-up-tables (LUT), which are usually built offline [25].

In the MPC framework, the DSVM is treated as a predictive controller with prediction horizon equal to the number of sub-periods. The discrete nature of the inverter switches positions implies that the MPC problem is nondetermistic Polynomial-time hard (NP-hard), i.e. it scales exponentially with the prediction horizon length. Proper solvers have been presented in literature to tackle this issue, such as the *branch and bound* and the *sphere decoding* methods [10]. The adoption of proper solvers is crucial to limit the computational effort at an affordable amounts. As an alternative, the selection of the optimal inverter switches position vector to be applied to the motor windings can be performed by exploiting both offline considerations and online optimisation, such as in [26]. The DSVM has been applied in several works, such as in [27] for an induction motor drives fed by a two-level inverter, or in [28] for grid-connected applications. In a nutshell, the DSVM is a software solution for increasing the number of equivalent voltage vector that the inverter can apply to the motor. Its hardware equivalent consists of a multilevel inverter, which may be too expensive for many applications.

Finding a proper tuning of the MPC for accomplishing both a reduced harmonic content and a low switching frequency could be a quite troublesome aspect [8]. Thus, many FS-MPC solutions in literature implement a *deadbeat* version of the algorithm, [29]. Deadbeat algorithms are also very popular in the area of model-based predictive controllers [29], [30].

The main contribution of the paper is the implementation of the DSVM technique to the motor parameter-free predictive current controller aiming at reducing the current ripple. The resulting architecture is an enhanced version of the adaptive controller proposed in [14]. The DSVM technique is a software stratagem which permits to increase the average switching frequency of the inverter [24] without modifying the hardware of the electric drive. The reduction of the current ripple contributes in reducing the Joule losses in the stator windings, thus increasing the efficiency of the overall system. A design procedure is provided to select the ratio between the sampling and the control frequency of the DSVM algorithm. A third contribution of the paper is the experimental comparison between model-based and parameter-free MPC methods in terms of current total harmonic distortion and average switching frequency, considering the entire motor speed range of operation. The two analysis were missing both in [14] and [15].

II. MOTOR PARAMETER-FREE CURRENTS PREDICTION

The conventional voltage balance equations of a synchronous motor in the synchronous *dq* reference frame is

$$\mathbf{u}_{dq} = R\mathbf{i}_{dq} + \begin{bmatrix} l_d & 0 \\ 0 & l_q \end{bmatrix} \frac{d\mathbf{i}_{dq}}{dt} + \omega_{\text{me}} \begin{bmatrix} 0 & -L_q \\ L_d & 0 \end{bmatrix} \mathbf{i}_{dq} + \mathbf{h}$$
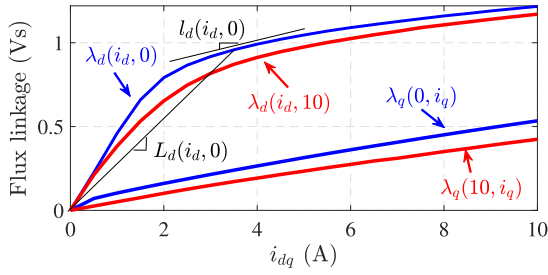
$$(1)$$

FIGURE 1. Magnetic flux linkages of a SyR motor at different currents and an example of *d*-axis apparent L_d and differential l_d inductances.

where $\mathbf{u}_{dq}$ and $\mathbf{i}_{dq}$ are the voltage and currents space vectors, respectively, R is the stator windings resistance, l_d and l_q are the incremental inductances, L_d and L_q are the apparent inductances, ω_e is the electric angular speed, $\mathbf{h} = [0 - \omega_e \Lambda_{pm}]^T$ is the back-electromotive force contribution due to the permanent magnet flux linkage Λ_{pm}, if present. The flux Λ_{pm} should be expressed as function of i_q to avoid a mathematical incongruousness when calculating the apparent inductances, see [2], whereas the resistance R varies with the temperature. The discrete state space representation is obtained from (1) by means of the forward Euler discretisation method, considering that a sufficiently small sampling time allows to obtain a fair representation of the currents dynamics. It yields:

$$\mathbf{i}_{dq}(k+1) = \mathbf{A}\mathbf{i}_{dq}(k) + \mathbf{B}\mathbf{h}(k) + \mathbf{B}\mathbf{u}_{dq}(k)$$

$$\mathbf{A} = \begin{bmatrix} 1 - \dfrac{RT_s}{l_d} & \dfrac{T_s\omega_e L_q}{l_d} \\ -\dfrac{T_s\omega_e L_d}{l_q} & 1 - \dfrac{T_s R}{l_q} \end{bmatrix}, \mathbf{B} = T_s \begin{bmatrix} \dfrac{1}{l_d} & 0 \\ 0 & \dfrac{1}{l_q} \end{bmatrix} \quad (2)$$

where T_s is the sampling period. For the sake of simplification, the speed ω_e is considered constant within one sampling period, which is an acceptable simplification when the sampling time is small with respect to the mechanical time constant. The voltage vector is obtained as $\mathbf{u}_{dq} = \mathbf{T}_P \mathbf{T}_c \mathbf{u}(k+1) u_{\text{bus}}$, where u_{bus} is the inverter bus input voltage. The 3×1 size vector $\mathbf{u}$ defines the switches positions, whose elements are in the set $\{0, 1\}$, $\mathbf{T}_C$ and $\mathbf{T}_P$ are the Clarke and Park transformations, respectively.

The current model (2) requires the accurate knowledge of the motor parameters. In particular, the nonlinear characteristics of the magnetic flux linkage with respect to $\mathbf{i}_{dq}$ are of utmost importance, since both the state matrix $\mathbf{A}$ and the input matrix $\mathbf{B}$ in (2) strongly depend from them. The typical flux characteristics of a synchronous reluctance motor, which is considered in this article, are reported in Fig. 1. A graphical interpretation of the incremental and apparent inductances is reported, too.

The current prediction at future steps can be obtained by means of (2). For instance, the current prediction at $(k+2)$ can be calculated as

$$\widehat{\mathbf{i}}_{dq}(k+2) = \mathbf{A}\mathbf{i}_{dq}(k+1) + \mathbf{B}\mathbf{u}_{dq}(k+1) + \mathbf{B}\mathbf{h}(k+1) \quad (3)$$

where the estimated voltage vector states $\mathbf{u}_{dq}(k+1)$ is the output of an optimisation algorithm as it will be described in Section III.

A. A RECURSIVE LEAST SQUARE APPROACH

The synchronous motor currents dynamics in (2) can be rewritten as follows:

$$\mathbf{i}_{dq}(k+1) = \mathbf{i}_{dq}(k) + (\mathbf{A} - \mathbf{I})\mathbf{i}_{dq}(k) + \mathbf{B}\mathbf{h}(k) + \mathbf{B}\mathbf{u}_{dq}(k) \quad (4)$$

where $\mathbf{I}$ is the 2×2 identity matrix. An equivalent model is derived from (4) suitable for online adaptation of the working point-dependent parameters. The method proposed in [14] adopts the following adaptive model:

$$\mathbf{i}_{dq}(k+1) = \mathbf{i}_{dq}(k) + \widehat{\mathbf{w}}(k) + \widehat{\mathbf{W}}(k)\mathbf{u}_{dq}(k)$$

$$\widehat{\mathbf{w}}(k) = \begin{bmatrix} p_{1,d} \\ p_{1,q} \end{bmatrix}, \ \widehat{\mathbf{W}}(k) = \begin{bmatrix} p_{2,d} & 0 \\ 0 & p_{2,q} \end{bmatrix} \quad (5)$$

where $p_{1,d}$, $p_{1,q}$, $p_{2,d}$ and $p_{2,q}$ are generic coefficients, not to be intended equivalent to the motor parameters of (2). The coefficients in (5) are estimated online by means of a recursive least square (RLS) algorithm. The standard algorithm consists of a set of equations that can be solved recursively:

$$\mathbf{G}(k) = \mathbf{Q}(k-1)\mathbf{\Phi}^T(k)(\mathbf{\Phi}(k)\mathbf{Q}(k-1)\mathbf{\Phi}^T(k) + f\mathbf{I})^{-1}$$

$$\widehat{\mathbf{p}}(k) = \widehat{\mathbf{p}}(k-1) + \mathbf{G}(k)(\mathbf{y}(k) - \mathbf{\Phi}(k)\widehat{\mathbf{p}}(k-1))$$

$$\mathbf{Q}(k) = \frac{1}{f}(\mathbf{Q}(k-1) - \mathbf{G}(k)\mathbf{\Phi}(k)\mathbf{Q}(k-1)). \quad (6)$$

The vector of measurements is

$$\mathbf{y}(k) = \begin{bmatrix} i_d(k) - i_d(k-1) \\ i_d(k-1) - i_d(k-2) \end{bmatrix} \text{ when } \widehat{\mathbf{p}}(k) = \begin{bmatrix} p_{1,d} \\ p_{2,d} \end{bmatrix} \quad (7)$$

because the identification of two coefficients, e.g. $[p_{1,d}; \ p_{2,d}]$, requires two independent set of measurements. A vector of measurements for the q-axis coefficients estimation can be obtained in the same fashion of (7) by replacing:

$$\mathbf{y}(k) = \begin{bmatrix} i_q(k) - i_q(k-1) \\ i_q(k-1) - i_q(k-2) \end{bmatrix} \text{ when } \widehat{\mathbf{p}}(k) = \begin{bmatrix} p_{1,q} \\ p_{2,q} \end{bmatrix} \quad (8)$$

Therefore, past currents and switches configurations are exploited to estimate all the coefficients, without resorting to motor parameter information. The regressors vector $\mathbf{\Phi}$ is $[1 \ u_d]^T$ when the d-axis coefficients are estimated by means of (6), or $[1 \ u_q]^T$ alternatively. The forgetting factor f can be chosen as reported in [14]. The gain matrix $\mathbf{G}(k)$ and the covariance matrix $\mathbf{Q}(k)$ are calculated at each time step (k) by the recursive least square algorithm. Finally, the vector $\widehat{\mathbf{w}}(k)$ is obtained by considering the first element of vector $\widehat{\mathbf{p}}(k)$ for each axis, whereas the two non-zero elements of matrix $\widehat{\mathbf{W}}(k)$ are obtained from the second element of vector $\widehat{\mathbf{p}}(k)$, again one for each axis. In order to avoid the resolution of a rank deficient least-square problem, the recursive least square algorithms work within a variable length time window (see [14] Section II-A).

The advantages that the proposed adaptive model brings along are manifold. First of all, the model (5) is general and it can be adopted for several synchronous motor topologies without additional commissioning effort. In other words, either permanent magnet and reluctance synchronous motors can be described by (5). The adaptive model modifies the coefficients values of $\widehat{\mathbf{W}}$ and $\widehat{\mathbf{w}}$ in (5) to track the synchronous motor model parameters variations. Thus, stator resistance and inductances variations are both taken into account. The adaptive model can replace, for instance, the use of LUTs for the inductances values, that are often included in the model-based MPC algorithm [31].

The current prediction at future time $k + 2$ can be calculated as follows

$$\widehat{\mathbf{i}}_{dq}(k+2) = \mathbf{i}_{dq}(k+1) + \widehat{\mathbf{w}}(k) + \widehat{\mathbf{W}}(k)\mathbf{u}_{dq}(k+1). \quad (9)$$

(9) can be used to predict current values at $k + 2 + n$, with $n \geq 1$, at the price of lower accuracy due to the constant value assumption of the coefficients value in $\widehat{\mathbf{w}}(k)$ and $\widehat{\mathbf{W}}(k)$. The adaptive model (5) relies on the coefficients adaptation to account for the innovation brought by the currents evolution.

III. DEADBEAT PREDICTIVE CURRENT CONTROL DESIGN

The main goal of the paper is to propose a deadbeat predictive current control algorithm performing a reduced current ripple compared to existing motor parameter-free algorithms. The control frequency should be kept at a low value for the sake of computational burden reduction. The switching frequency is a consequence of the adopted switches state updating frequency, which is selected to be a fraction of the control frequency. Therefore, two different time scales are introduced to distinguish between *control* and *switches* state updating frequency. The former is denoted by the time index k_c, whereas the latter by k_s. The equivalent control period T_c is selected as an integer multiple of the switches state update period T_s. An example of the different time variables is reported in Fig. 2, where a ratio $T_c/T_s = N = 3$ was selected for the sake of a clearer representation. The choice of N will be discussed in Section IV-A.

In order to minimise the tracking error, a quadratic cost function is adopted in this paper. A detailed overview of alternative cost functions formulation are reported in [8]. It is worth pointing out that alternative finite-set MPC cost-functions might yield a lower value for a particular figure of merit, e.g. the number of switching events, at the expense of an increment in others, e.g. the current harmonic content. A prediction horizon N is used to exploit the adaptive model (5)

$$\min_{\mathbf{u}(\cdot)} \quad \sum_{z=1}^{N} \|\mathbf{i}_{dq}^* - \mathbf{i}_{dq}(k_s + z)\|^2$$

$$\text{s.t.} \quad \mathbf{i}_{dq}(k_s+1) = \mathbf{i}_{dq}(k_s) + \widehat{\mathbf{W}}\mathbf{u}_{dq}(k_s) + \widehat{\mathbf{w}}(k_s) \quad (10)$$

For the sake of tuning simplicity, no additional cost figures have been added rather than the current tracking.
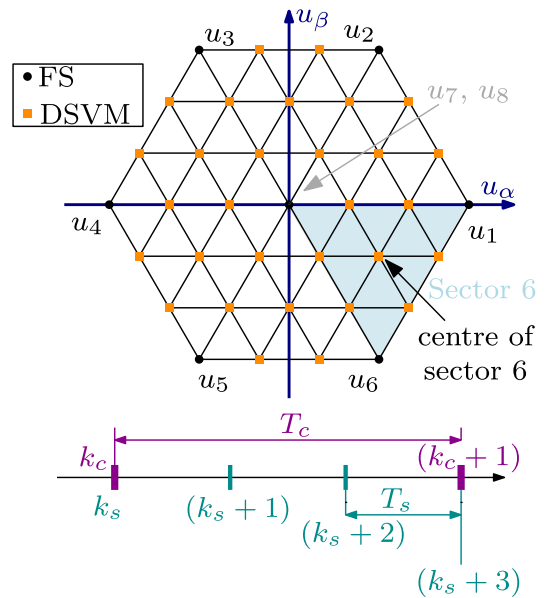

FIGURE 2. Set of $\alpha\beta$ voltage vectors that can be synthesised using a standard FS controller and the DSVM method.

In turn, the solution of (10) consists of a sequence of switches configurations. In the original parameter-free controller [16], the receding horizon policy was adopted. Thus, the optimisation problem is solved for every sampling period T_s. It is worth reminding that a digital delay of one control step occurs between the computation of the optimal control action and its application. The delay is compensated by means of an open loop prediction, as described in [10].

A. DSVM APPLICATION TO THE MOTOR PARAMETER-FREE CONTROLLER

A three-phase two level inverter can generate only eight base voltage vectors in the $\alpha\beta$ stator reference frame, corresponding to the eight possible configurations of inverter switch positions. Hereinafter these vectors are denoted as: $u_1 = [1\,0\,0]^T$, $u_2 = [1\,1\,0]^T$, $u_3 = [0\,1\,0]^T$, $u_4 = [0\,1\,1]^T$, $u_5 = [0\,0\,1]^T$, $u_6 = [1\,0\,1]^T$, $u_7 = [0\,0\,0]^T$ and $u_8 = [1\,1\,1]^T$. The fundamental vectors are reported in Fig. 2 by means of black dots. It is worth noticing that a zero voltage vector can be generated by two switches configurations, i.e u_7 and u_8: the choice between the two of them is driven by the minimisation of switching events.

According to the DSVM, the control period T_c is divided in an integer number of shorter sub-period T_s. Different base voltage vectors can be potentially applied at each one of these T_s-long sub-periods. From a predictive controller point of view, the MPC problem solution is calculated at every T_c. The RLS algorithm described in Section II-A is run with a period T_s to better track the coefficients $\widehat{\mathbf{p}}$ evolution. In other words, the time variable k from (4) to (9) should be rewritten by using the time variable k_s. Therefore, the validity of equations (4)-(9) is general for any value of N.
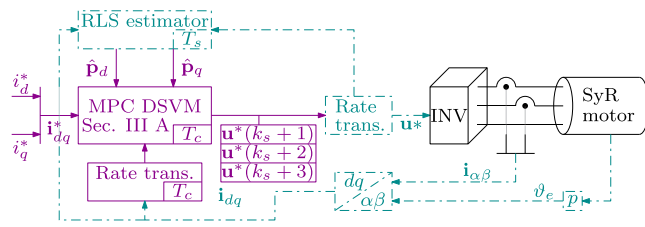
FIGURE 3. Overview of the control scheme architecture. Continuous-line (magenta) and dashed-line (cyan) indicate the T_c and T_s samples times, respectively.

For the sake of simplicity, it is convenient to set the prediction horizon length N equal to the number of sub-periods. The different sample rates of the main blocks that compose the proposed control scheme are sketched in Fig. 3. As a result, the DSVM enlarges the set of equivalent voltages that can be synthesised within a control period T_c. The augmented set of voltages is represented by orange squares in Fig. 2, where a number of sub-periods $N = 3$ was chosen.

As the number of sub-periods N increases, problem (10) becomes more and more computationally expensive. In fact, the number of equivalent vectors grows in an exponential rate, and so does the number of cost function evaluations. Moreover, each equivalent voltage vector can be obtained with different combinations of the base vectors $u_1, \ldots, u_8$. The proposed deadbeat motor parameter-free predictive controller adopts one of the most up-to-dated methods to solve the control problem, i.e. the one proposed in [26]. The idea behind this method is to separate the current tracking problem (10) from the selection of the optimal combination of base voltages.

The tracking problem is solved very efficiently in terms of the equivalent voltage vector. In fact, the cost function is first evaluated for the six central voltages of the hexagon sectors. An example of sector and its centre is reported in Fig. 2, in particular *sector 6*. Once the voltage vector returning the lowest cost is found, all other vectors that belong to the same sector are evaluated. Considering 3 sub-periods, 15 cost evaluations are computed, instead of evaluating all the 37 equivalent vectors. This number is obtained by considering the sectors centres, i.e. 6, the number of voltage vectors in the sector, i.e. 8, and only one zero voltage vector. Then, the voltage vector of the remaining set returning the lowest cost is considered and it is synthesised in such a way that the number of inverter switches commutations is minimised. The minimisation of the switching events is computationally cheap due to offline considerations (maximum 4 cases need to be considered). Extensive considerations and detailed discussions are reported in [26]. The idea of separating the tracking problem from the switching minimisation can be extended to a different number of sub-periods. A flow chart of the overall deadbeat parameter-free algorithm is reported in Fig. 4. The distinctive features with respect to the previous works of the authors [14], [16] are highlighted. The proposed paper reports several implementation hints which comes from the results discussions in Sect. IV.
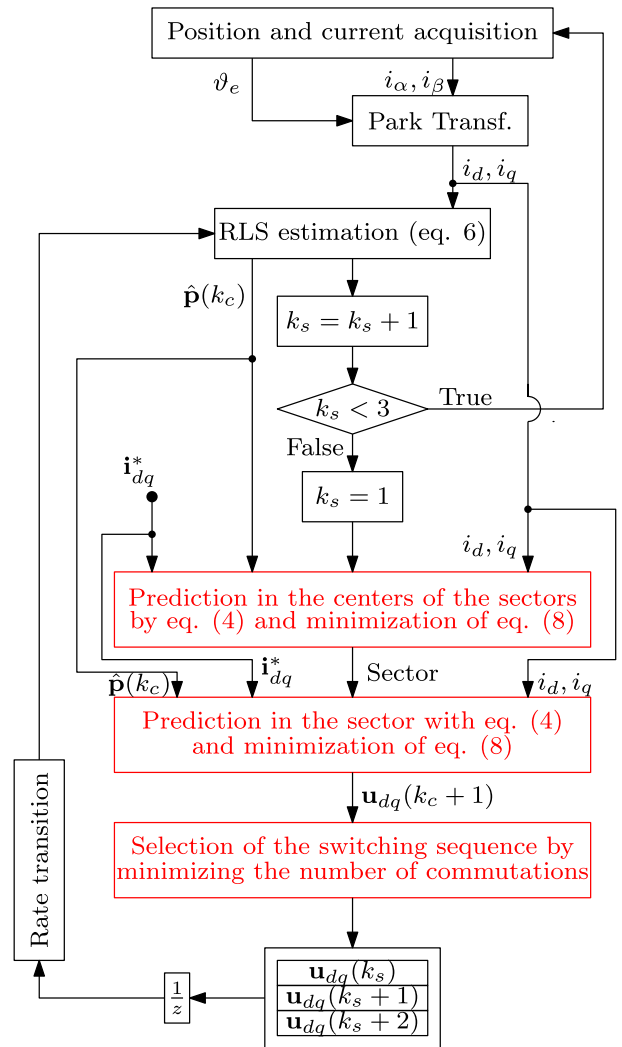

FIGURE 4. Flow chart of the DSVM parameter-free MPC ($N = 3$).

TABLE I Parameters of the Prototype SyR Motor Under Test

Motor Data	Symbol	Values
Pole pairs	p	2
Phase resistance	R	$4.6\,\Omega$
d-axis inductance (unsaturated)	L_d	$0.25\,\mathrm{H}$
q-axis inductance (unsaturated)	L_q	$0.08\,\mathrm{H}$
Nominal current	I_N	$8.5\,\mathrm{A}$
Nominal d-axis current	$I_{d,N}$	$3.6\,\mathrm{A}$
Nominal q-axis current	$I_{q,N}$	$7.7\,\mathrm{A}$
Nominal speed	Ω_N	$500\,\mathrm{rpm}$

IV. EXPERIMENTAL RESULTS AND DISCUSSION

The motor under test was a SyR motor, whose plate parameters are reported in Table I. A dSPACE MicroLabBox hardware was used for the real-time implementation, featuring a 2 GHz NXP QorIQ P5020 microprocessor. The test rig is reported in Fig. 5. The inverter bus voltage was set at $u_{\mathrm{bus}} = 300\,\mathrm{V}$. The SyR motor under test was dragged by a
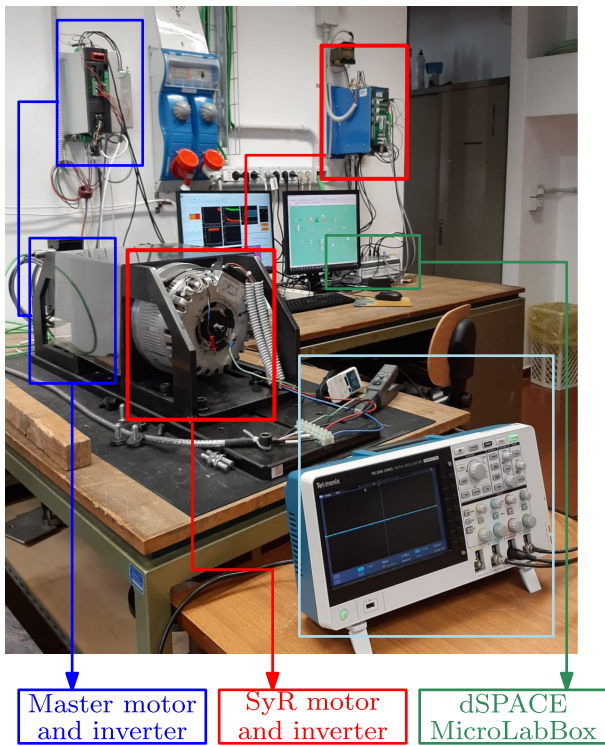
FIGURE 5. Test rig layout.

Master motor and inverter | SyR motor and inverter | dSPACE MicroLabBox

FIGURE 6. Switching frequency and current THD as function of the number of sub-periods of the DSVM.

the more accurate model. Finally, the novel DSVM controller based on the parameter-free algorithm proposed in this paper was tested and compared to the previous alternatives.

All the quantities reported in the results are normalised with respect to their nominal value, reported in Table I.

A. SELECTION OF THE NUMBER OF SUB-PERIODS

The only parameter that needs to be selected when implementing the parameter-free DSVM algorithm is the number of sub-periods within one control period. This parameter was selected by means of a commissioning test of the SyR motor at its nominal operating point (Table I). Four different number of sub-periods were analysed.

The average switching frequency of the inverter and the Total Harmonic Distortion (THD) of the phase currents were monitored during the commissioning. On the one hand, the average switching frequency reflects the losses due to the switching. The average switching frequency was measured starting from the switches states generated by the controller implemented in the dSPACE hardware. On the other hand, currents THD is selected as performance index to prove and quantify the current ripple reduction. Indeed, THD is the most adopted index by practitioners and the most widespread in literature. A lower THD results in reduced Joule losses in the stator windings and a lower torque ripple. Phase currents THD was measured by means of current probes and an oscilloscope (Fig. 5). All the results are reported in Fig. 6.

The two considered performance indexes conflicts when the number of sub-periods increases. In particular, the switching frequency grows with the number of sub-periods, while the current THD has an opposite trend. After the commissioning test, the design of the controller can be carried out harmonising it with the requirements of the application. In this paper, it is selected a number of sub-periods equal to three, since the main scope of this work is to minimise the current THD. Indeed, choosing four sub-periods allows a small reduction of the ripple at a price of a relevant increase of the switching. It is worth highlighting that the proposed model-free algorithm is capable of self-adapting the coefficients $\widehat{\mathbf{p}}$ for any number of sub-periods. Therefore, the number of sub-periods can be varied even during online operations thanks to the adaptability characteristics of the proposed model-free solution, provided that sufficient computational power is available. All the results reported hereinafter regarding DSVM based algorithms

speed-controlled PMSM load motor during all tests reported in this Section.

Six control schemes were compared, three FS-MPC algorithms and three DSVM based predictive control algorithms. Model-based control schemes, i.e. the ones that adopt the parametric model of the PMSM (2), are denoted with the acronym MB. The sampling frequency of the finite-set algorithms was $f_s = 10$ kHz and it coincided with the control frequency. The DSVM schemes shared the same control frequency of the FS ones. However, they differed in terms of sampling frequency, which is three times higher ($N = 3$), if not specified. It is worth recalling that the oversampling was exploited by the RLS estimators to update the parameter-free adaptive model. No tuning parameters are requested in (10) for the predictive controllers. A forgetting factor $f = 0.98$ was selected in (6), following the design guidelines discussed in [14]. In conclusion, the only remaining parameter that has to be selected is the number of sub-periods, as discussed in Section IV-A.

Two model-based MPC scheme were implemented. One exploited the nominal motor parameters for the current prediction, whereas the other a more accurate model. The model was designed to take into account the effects of the iron-saturation. Moreover, a third FS controller was implemented, i.e. the deadbeat version of the parameter-free method proposed in [14]. On the other hand, two model-based MPC schemes adopting a DSVM architecture were implemented for the sake of comparison. As for the FS case, one scheme implemented the nominal motor model, whereas the other one
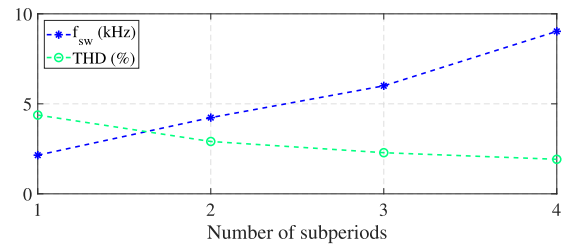
TABLE II Average Turn-Around-Time of the Considered Controllers for Different Number of Sub-Periods *N*

N	MB	MB + LUT parameters	parameter-free
1	$10\,\mu s$	$13.6\,\mu s$	$13.7\,\mu s$
2	$10.6\,\mu s$	$14.3\,\mu s$	$14.3\,\mu s$
3	$12\,\mu s$	$15.5\,\mu s$	$15.5\,\mu s$
4	$12.6\,\mu s$	$16.4\,\mu s$	$16.5\,\mu s$

adopts three sub-periods, which results in a sampling frequency of 30 kHz.

From practitioners point of view, it is of primary interest to know whether the computational burden of the designed deadbeat controller is higher than the one of a benchmark FS controller with receding horizon running at 30 kHz. On the one hand, a FS controller would solve $N = 3$ times the MPC optimisation problem by evaluating the 8 base voltages reported in Fig. 2. It results cheaper to evaluate 7 base voltages, thus considering the two zero vectors u_7 and u_8 together. Then, if a zero vector is optimal, the one that involves the minimum switching effort is applied. In conclusion, the cost function is evaluated 21 times every T_c. On the other hand, the proposed deadbeat parameter-free method requires 15 cost evaluations every T_c, as already discussed in Section III-A. Thus, a lower number of cost evaluations is achieved with respect to a conventional FS controller. Nevertheless, the computation time required to identify the optimal switching pattern increases by the number of sub-periods.

In general, it is difficult to state which solution is computationally cheaper, since it depends on the adopted hardware and on the code generation procedure, too. Therefore, the average turn-around-time of the controller for several number of sub-periods is reported in Table II, as comprehensive computational burden index. This is a common choice for evaluating the computational complexity of a predictive control algorithm, such as in [32], [33]. It is worth noting that the proposed parameter-free scheme guarantees a computation time similar to the one of a model-based MPC which adopts an accurate motor model.

B. ANALYSIS OF THE PHASE CURRENT DISTORTION

The main motivation for combining the DSVM method with the parameter-free scheme is to reduce the ripple in the motor currents. Therefore, several tests were performed in order to analyse the ripple in the entire operating speed range of the SyR motor, considering all the six predictive controllers implemented in the paper. The results are reported in Fig. 7, categorised according to the type of modulation technique used (FS or DSVM).

As a first consideration, the current THD obtained using the DSVM technique (Fig. 7(a)) is always lower than the one obtained with the FS method (Fig. 7(b)), regardless of the working speed and the predictive control algorithm. Indeed,
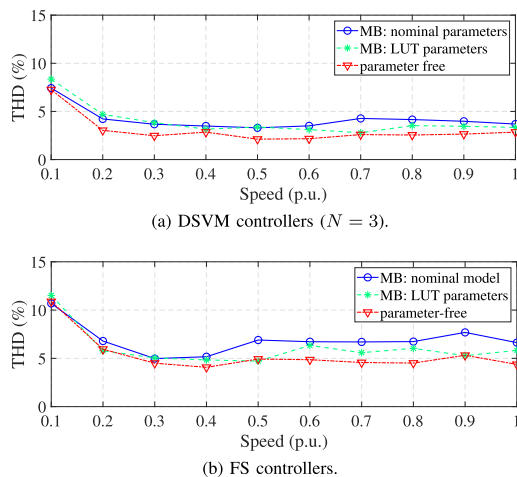
FIGURE 7. Comparison of the current THD of the different controllers for different operating speeds.

this is a well known result in literature [29]. Moreover, the model-based algorithms that exploit a more accurate model outperform the ones that implement just the nominal model, regardless of the adopted modulation technique.

The current THD analysis for the parameter-free algorithms is definitely an original contribution of this work. The parameter-free schemes achieve a current THD which is equal or lower than their model-based counterparts within the whole considered speed range. This may be justified by the fact that even the SyR motor model that accounts for the iron saturation does not fully describe the dynamics of the currents. It is worth highlighting, indeed, that the proposed accurate model could neglect some non-linear phenomena. The authors are aware that these phenomena may be included in the motor model. However, an even more accurate model requires additional commissioning effort. Moreover, the current predictions evaluations become more computationally expensive. Therefore, the simple parameter-free adaptive model appears to be a reasonable compromise between having good performances in terms of currents THD and maintaining a relatively cheap prediction model.

The phase currents are reported for two particular operating speed in Fig. 8, for sake of completeness. The parameter-free schemes are compared to the model-based algorithms that use the more accurate motor model. The phase shift between the current measurements is introduced on purpose for the sake of clarity. The current ripple reduction obtained thanks to the DSVM methods Fig. 8(a)-8(b) with respect to the FS ones Fig. 8(c)-8(d) is evident. The improvement in the waveform is achieved especially in the peaks of the sine curve, where low current derivatives are required. In fact, the DSVM unlocks the possibility of synthesising voltage vectors of lower magnitude (see Fig. 2). Thus, the current variations become smoother, as can be mathematically proved by means of (2).

In order to provide quantitative results, some relevant motor operating points are considered, as shown by the grid reported
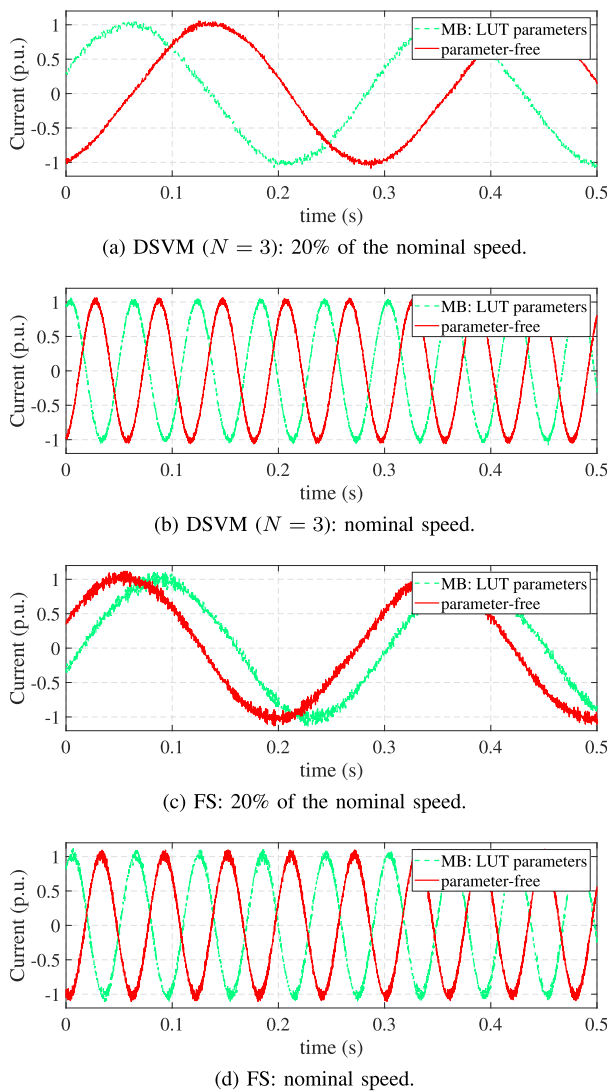
(a) DSVM ($N = 3$): 20% of the nominal speed.

(b) DSVM ($N = 3$): nominal speed.

(c) FS: 20% of the nominal speed.

(d) FS: nominal speed.

FIGURE 8. Motor phase current at steady state for two operating speed and considering different control strategies.

FIGURE 9. Map of the analysed points. Squares denote the points suggested by the EN 50598-2 standard. The considered points are red-coloured.

TABLE III THD (%) Comparison Between the Three Controllers, Considering the Red Points of Fig. 9

Point	parameter-free	MB	η	MB + LUT	η
P1	5.7	8.2	-31	6.9	-18.1
P2	3.6	5.8	-37	3.9	-5.7
P3	3.0	4.9	-39	3.2	-5.9
P4	6.0	8.7	-31	6.9	-13.4
P5	3.8	6.0	-37	3.8	-0.5
P6	2.7	4.6	-42	2.9	-7.0
P7	6.9	8.9	-22	7.2	-3.8
P8	3.8	6.1	-37	4.1	-5.7
P9	2.6	4.4	-41	2.6	-1.9

Joule losses reduction compared to a model-based solution with constant parameters.

C. ANALYSIS OF THE SWITCHING FREQUENCY

The DSVM technique permits a reduction of the current THD at a price of an increase of the average inverter switching frequency. For this reason, the current THD analysis performed in the section above is supported by an analysis of the average inverter switching frequency f_{sw}, reported in Fig. 10.

All the DSVM based control algorithms (Fig. 10(a)) produce a switching frequency on average higher with respect to the FS ones (Fig. 10(b)). This is, in general, a good initial results. The implemented DSVM algorithms, characterised by 3 sub-periods, allow a maximum switching frequency three times higher than the FS ones. Thus, the frequency is increased less than linearly. Moreover, it is noticed that the switching frequency of the FS algorithms always decreases when increasing operating speeds. This is mainly due to the fact that the motional cross-coupling term in (2) is proportional to the speed. Thus, in steady state condition, the current derivatives are lower at high speed, when the cross coupling counterbalances the input voltage term, reducing the overall available voltage.

As for the THD analysis, the model based controller that takes into account the saturation in the iron results as the best between the model based solutions. However, the parameter-free paradigm grants a slightly lower switching effort than the model-based one. The most relevant improvements are

in Fig. 9. The selected points are similar to the ones suggested by the EN50598-2 standard, which regards the efficiency evaluation of the drive system. The obtained THD results are reported in Table III for each point of the grid. The proposed parameter-free method exhibits promising results with respect to the model-based MPC. The percentage improvements of the current THD achieved by the proposed technique can be calculated as

$$\eta = \left(1 - \frac{THD_{\text{MB}} - THD_{\text{MF}}}{THD_{\text{MB}}} \right) \cdot 100 \qquad (11)$$

The results in terms of THD differences are reported in Table III. From the efficiency point of view, the reduction of current THD is proportional to the reduction of Joule losses cause by the additional harmonics components of the motor currents. The results of Table III confirms that the proposed model-free algorithm consists a remarkable improvement of
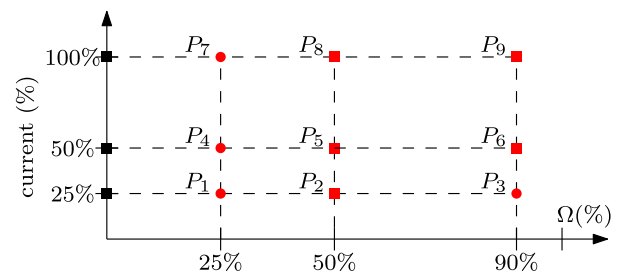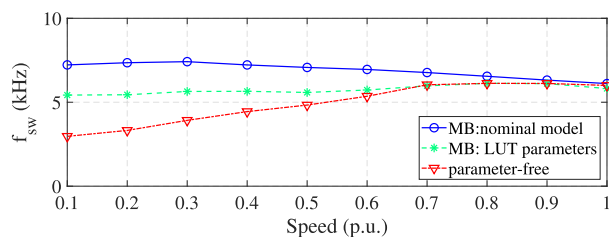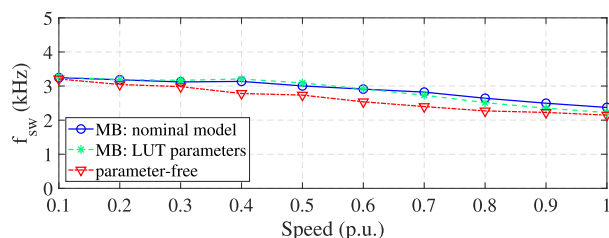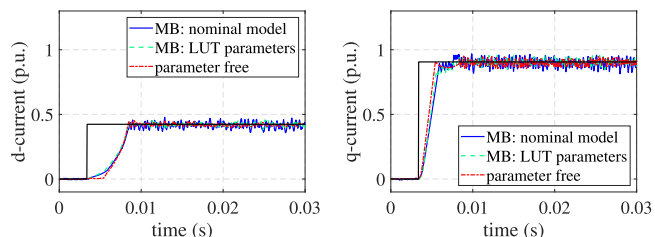
(a) DSVM controllers ($N = 3$).

(b) FS controllers.

FIGURE 10. Comparison of the switching frequency among the different controllers for different operating speed.

(a) d-axis current: standstill.

(b) q-axis current: standstill.

(c) d-axis current: nominal speed.

(d) q-axis current: nominal speed.

FIGURE 11. Comparison of the step responses among the DSVM model-based and parameter-free controllers at different speed.

TABLE IV Switching Frequency (kHz) Comparison Between the Three Controllers, Considering the Red Points of Fig. 9
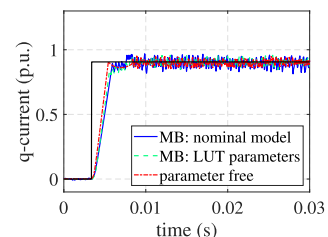
Point	parameter-free	MB	η	MB + LUT	η
P1	6	6.7	-11	6.1	-1.6
P2	2.7	7.4	-64	4.0	-34
P3	3.5	7.1	-51	4.9	-28.4
P4	4.7	7.2	-35	5.8	-19.2
P5	4.6	7.3	-38	5.1	-11.4
P6	4.4	6.8	-35	5.0	-12.7
P7	6.2	7.1	-13	6.2	-0.2
P8	5.2	5.9	-12	5.5	-5.1
P9	5.8	6.1	-5	5.8	-0.2

FIGURE 12. Estimated coefficients dynamics vs current dynamic.

achieved by the DSVM parameter-free algorithm at low speed (Fig. 10(a)). In conclusion, the currents THD and switching frequency analysis of the controllers highlights some beneficial effects of the DSVM parameter-free approach. In fact, it permits a significant reduction of the phase current harmonic content and, at the same time, the lower increase of switching frequency between the DSVM based controllers.
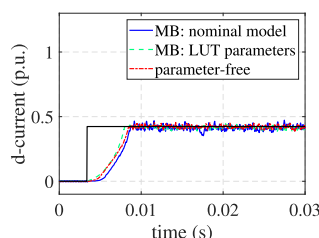
Quantitative results are reported in Table IV. They were obtained by considering the working points defined in Fig. 9. The switching frequency plays an important role in the drive efficiency, which may depend on the size of the drive and on the technology of the inverter switches. Anyway, switching losses are always proportional to the average switching frequency of the converter. The results reported in Table IV suggest that the proposed solution allows to obtain lower switching frequencies than the model-based solution with constant parameters. Actually, the switching frequencies of the proposed model-free solution are very similar to the ones of the model-based algorithm with LUT parameters, i.e. with the correct model for each working point. Lower losses in the
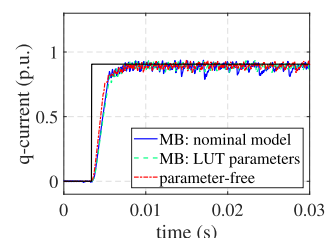
converter improve both the design of the cooling system and the life-cycles of the switches.

D. STEP RESPONSE ANALYSIS

The currents reference step responses are considered here to analyse the dynamic performances of the proposed DSVM parameter-free controller. All the tests are performed changing the current references step-wise from zero to the nominal point Fig. 11- 13. The dynamics are repeated for two operating speed, namely at standstill and at nominal speed, covering the entire working range of the motor. The currents shape characteristics of Fig. 11 and 13 resemble the magnetic curve relationships of Fig. 1. As a distinctive feature of every finite-set algorithm, the transient responses are as fast as possible subject to the available voltage.

From the rise time and overshoot point of view, all the algorithms assure very good performances and are very similar between all the schemes. This is, in fact, a distinguished feature of the MPC paradigm. It is worth noticing that the parameter-free exhibits a similar dynamic behaviour of a model based scheme, without any a priori information of the motor parameter. However, the model-based controllers that

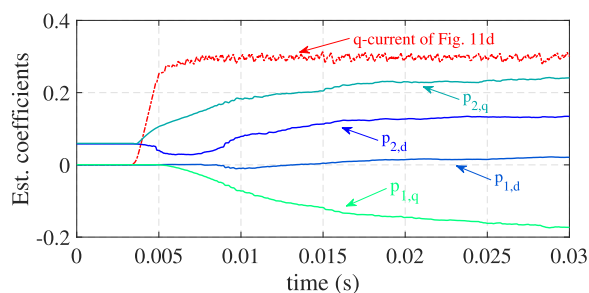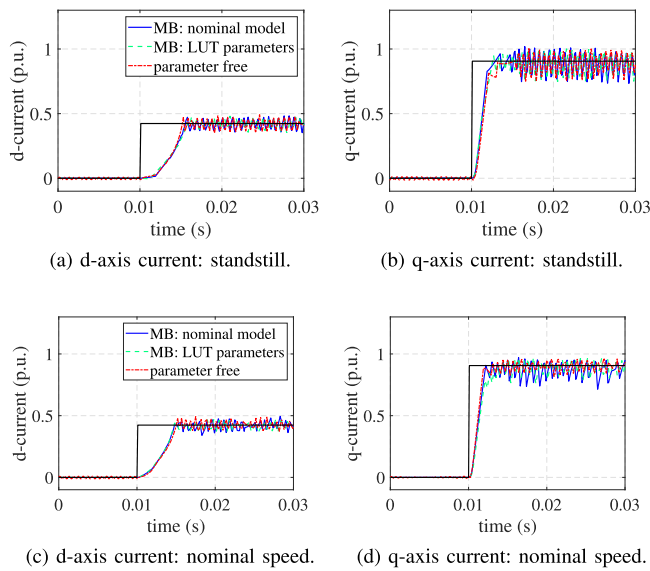(a) d-axis current: standstill.

(b) q-axis current: standstill.

(c) d-axis current: nominal speed.

(d) q-axis current: nominal speed.

FIGURE 13. Comparison of the step responses among the FS model-based and parameter-free controllers at different speed.

adopt an accurate motor model tend to behave slightly better. In case of the parameter-free algorithms, in fact, the model learning rate is determined by the recursive least square estimator dynamics. The dynamics of the estimated coefficients during the step responses in Fig. 11 are reported in Fig. 12. The currents responses are faster than the estimators ones. Thus, the parameter-free controller is adapting the model during the transients, while the accurate model-based controller exploits previously measured motor-parameters. This fact justifies the minimal reduction of performances of the parameter-free controller in terms of step response when compared to accurate model-based schemes. Nevertheless, the steady-state current ripple improvement achieved with the parameter-free approach counterbalance the limited reduction of dynamic performances. The beneficial effects of the adapted coefficients on the current ripple is thus a reduction of the THD as discussed in Sect. IV-B, which are comparable to a model-based predictive current control algorithm with LUTs based parameters.

V. CONCLUSION

A motor parameter-free predictive current controller coupled with a discrete space vector modulation technique is proposed in this paper. The motivations behind this design are manifold. First, the implementation of recursive least square estimators carries along the real time adaptation of the prediction model. The discrete space vector modulation permits a reduction of the current ripple that affects the parameter-free algorithm, with respect to the finite-set version. This, in turn, allows to reduce Joule losses in the stator windings, increasing the efficiency of the drive. Finally, thanks to the deadbeat implementation of the predictive control algorithm, the number of tuning parameters of the proposed algorithm is minimal. In particular, no motor characterisation are required and only one

commissioning test is needed to tune properly the number of sub-periods of the discrete space vector modulation.

The experimental results included in the work permits to address the design of the only tuning parameter. Thanks to the proposed commissioning test, a suitable number of sub-periods of the discrete space vector modulation can be selected according to the specific application. The total phase current distortion and the inverter average switching frequency are discussed by means of ad-hoc tests. The price paid to implement a computationally heavier algorithm is worthy. In fact, the proposed parameter-free discrete space vector modulation algorithm has a lower current distortion with respect to the finite set version. The method outperforms even model based ones in some operating points. Finally, the analysis of the dynamic performances of the proposed scheme is provided, too. The proposed method behaves similarly than equivalent model-based schemes, characterised by accurate prediction models obtained through many commissioning tests. At the end, the impressive feature of the proposed algorithm is that it emulates, sometimes outperforming, the behaviour of model-based controllers, but dribbling all the overwhelming critical issues related to the model identification.

REFERENCES

[1] P. Karamanakos, E. Liegmann, T. Geyer, and R. Kennel, "Model predictive control of power electronic systems: Methods, results, and challenges," *IEEE Open J. Ind. Appl.*, vol. 1, pp. 95–114, Aug. 2020, doi: 10.1109/OJIA.2020.3020184.

[2] G. Pellegrino, T. M. Jahns, N. Bianchi, W. Soong, and F. Cupertino, *The Rediscovery of Synchronous Reluctance and Ferrite Permanent Magnet Motors*, 1st ed. Berlin, Germany: Springer, 2016.

[3] S. Bolognani, S. Bolognani, L. Peretti, and M. Zigliotto, "Design and implementation of model predictive control for electrical motor drives," *IEEE Trans. Ind. Electron.*, vol. 56, no. 6, pp. 1925–1936, Jun. 2009.

[4] M. Jofré, A. M. Llor, and C. A. Silva, "Sensorless low switching frequency explicit model predictive control of induction machines fed by neutral point clamped inverter," *IEEE Trans. Ind. Electron.*, vol. 66, no. 12, pp. 9122–9128, Dec. 2019.

[5] M. Preindl and S. Bolognani, "Comparison of direct and PWM model predictive control for power electronic and drive systems," in *Proc. 28th Annu. IEEE Appl. Power Electron. Conf. Expo.*, 2013, pp. 2526–2533.

[6] S. Hanke, O. Wallscheid, and J. Böcker, "Continuous-control-set model predictive control with integrated modulator in permanent magnet synchronous motor applications," in *Proc. IEEE Int. Electric Mach. Drives Conf.*, 2019, pp. 2210–2216.

[7] F. Wang, X. Mei, J. Rodriguez, and R. Kennel, "Model predictive control for electrical drive systems-an overview," *CES Trans. Elect. Mach. Syst.*, vol. 1, no. 3, pp. 219–230, 2017.

[8] P. Karamanakos and T. Geyer, "Guidelines for the design of finite control set model predictive controllers," *IEEE Trans. Power Electron.*, vol. 35, no. 7, pp. 7434–7450, Jul. 2020.

[9] T. Dragičević and M. Novak, "Weighting factor design in model predictive control of power electronic converters: An artificial neural network approach," *IEEE Trans. Ind. Electron.*, vol. 66, no. 11, pp. 8870–8880, Nov. 2019.

[10] T. Geyer, *Model Predictive Control of High Power Converters and Industrial Drives*. Hoboken, NJ, USA: Wiley, 2016.

[11] L. Ortombina, D. Pasqualotto, F. Tinazzi, and M. Zigliotto, "Magnetic model identification of synchronous motors considering speed and load transients," *IEEE Trans. Ind. Appl.*, vol. 56, no. 5, pp. 4945–4954, Sep./Oct. 2020.

[12] S. A. Odhano, P. Pescetto, H. A. A. Awan, M. Hinkkanen, G. Pellegrino, and R. Bojoi, "Parameter identification and self-commissioning in AC motor drives: A technology status review," *IEEE Trans. Power Electron.*, vol. 34, no. 4, pp. 3603–3614, Apr. 2019.

[13] A. Brosch, S. Hanke, O. Wallscheid, and J. Böcker, "Data-driven recursive least squares estimation for model predictive current control of permanent magnet synchronous motors," *IEEE Trans. Power Electron.*, vol. 36, no. 2, pp. 2179–2190, Feb. 2021.

[14] F. Tinazzi, P. G. Carlet, S. Bolognani, and M. Zigliotto, "Motor parameter-free predictive current control of synchronous motors by recursive least square self-commissioning model," *IEEE Trans. Ind. Electron.*, vol. 67, no. 11, pp. 9093–9100, Nov. 2020.

[15] C. Lin, J. Yu, Y. Lai, and H. Yu, "Improved model-free predictive current control for synchronous reluctance motor drives," *IEEE Trans. Ind. Electron.*, vol. 63, no. 6, pp. 3942–3953, Jun. 2016.

[16] P. G. Carlet, F. Tinazzi, S. Bolognani, and M. Zigliotto, "An effective model-free predictive current control for synchronous reluctance motor drives," *IEEE Trans. Ind. Appl.*, vol. 55, no. 4, pp. 3781–3790, Jul./Aug. 2019.

[17] R. Heydari, H. Young, Z. Rafiee, F. Flores-Bahamonde, M. Savaghebi, and J. Rodriguez, "Model-free predictive current control of a voltage source inverter based on identification algorithm," in *Proc. 46th Annu. Conf. IEEE Ind. Electron. Soc.*, 2020, pp. 3065–3070.

[18] L. Xu, G. Chen, and Q. Li, "Ultra-local model-free predictive current control based on nonlinear disturbance compensation for permanent magnet synchronous motor," *IEEE Access*, vol. 8, pp. 127690–127699, 2020, doi: 10.1109/ACCESS.2020.3008158.

[19] Y. Zhang, J. Jin, and L. Huang, "Model-free predictive current control of PMSM drives based on extended state observer using ultralocal model," *IEEE Trans. Ind. Electron.*, vol. 68, no. 2, pp. 993–1003, Feb. 2021.

[20] J. Rodríguez, R. Heydari, Z. Rafiee, H. A. Young, F. Flores-Bahamonde, and M. Shahparasti, "Model-free predictive current control of a voltage source inverter," *IEEE Access*, vol. 8, pp. 211104–211114, 2020, doi: 10.1109/ACCESS.2020.3039050.

[21] M. S. Mousavi, S. Alireza Davari, V. Nekoukar, C. Garcia, and J. Rodriguez, "Model-free finite set predictive voltage control of induction motor," in *Proc. 12th Power Electron. Drive Syst. Technol. Conf.*, 2021, pp. 1–5.

[22] Y. Zhang, L. Bingyu, J. Liu, and X. Liu, "Model-free predictive current control of PWM rectifier under unbalanced and distorted network," in *Proc. IEEE Energy Convers. Congr. Expo.*, 2020, pp. 5944–5951.

[23] P. G. Ipoum-Ngome, D. L. Mon-Nzongo, R. C. C. Flesch, J. Song-Manguelle, M. Wang, and T. Jin, "Model-free predictive current control for multilevel voltage source inverters," *IEEE Trans. Ind. Electron.*, vol. 68, no. 10, pp. 9984–9997, Oct. 2021.

[24] D. Casadei, G. Serra, and K. Tani, "Implementation of a direct control algorithm for induction motors based on discrete space vector modulation," *IEEE Trans. Power Electron.*, vol. 15, no. 4, pp. 769–777, Jul. 2000.

[25] Y. Zhang, H. Jiang, and H. Yang, "A universal discrete space vector modulation based model predictive control for PMSM drives," in *Proc. 22nd Int. Conf. Elect. Mach. Syst.*, 2019, pp. 1–6.

[26] I. Osman, D. Xiao, M. F. Rahman, M. Norambuena, and J. Rodriguez, "Discrete space vector modulation based model predictive flux control with reduced switching frequency for IM drive," *IEEE Trans. Energy Convers.*, vol. 36, no. 2, pp. 1357–1367, Jun. 2021.

[27] I. Osman, D. Xiao, K. S. Alam, S. M. S. I. Shakib, M. P. Akter, and M. F. Rahman, "Discrete space vector modulation-based model predictive torque control with no suboptimization," *IEEE Trans. Ind. Electron.*, vol. 67, no. 10, pp. 8164–8174, Oct. 2020.

[28] H.-C. Moon, J.-S. Lee, and K.-B. Lee, "A robust deadbeat finite set model predictive current control based on discrete space vector modulation for a grid-connected voltage source inverter," *IEEE Trans. Energy Convers.*, vol. 33, no. 4, pp. 1719–1728, Dec. 2018.

[29] Y. Wang *et al.*, "Deadbeat model-predictive torque control with discrete space-vector modulation for PMSM drives," *IEEE Trans. Ind. Electron.*, vol. 64, no. 5, pp. 3537–3547, May 2017.

[30] Y. Zhang, Y. Bai, and H. Yang, "A universal multiple-vector-based model predictive control of induction motor drives," *IEEE Trans. Power Electron.*, vol. 33, no. 8, pp. 6957–6969, Aug. 2018.

[31] S. Vazquez, J. Rodriguez, M. Rivera, L. G. Franquelo, and M. Norambuena, "Model predictive control for power converters and drives: Advances and trends," *IEEE Trans. Ind. Electron.*, vol. 64, no. 2, pp. 935–947, Feb. 2017.

[32] P. Acuna, C. A. Rojas, R. Baidya, R. P. Aguilera, and J. E. Fletcher, "On the impact of transients on multistep model predictive control for medium-voltage drives," *IEEE Trans. Power Electron.*, vol. 34, no. 9, pp. 8342–8355, Sep. 2019.

[33] A. Zanelli, J. Kullick, H. M. Eldeeb, G. Frison, C. M. Hackl, and M. Diehl, "Continuous control set nonlinear model predictive control of reluctance synchronous machines," *IEEE Trans. Control Syst. Technol.*, to be published, doi: 10.1109/TCST.2020.3043956.

SILVERIO BOLOGNANI (Fellow, IEEE) received the Laurea degree in electrical engineering from the University of Padova, Italy, in 1976. In the same year, he joined the Department of Electrical Engineering of that University, where he was involved in the analysis and design of thyristor converters and synchronous motor drives. Successively he has carried out research activities about the design and control of motor drives for land and marine propulsion, energy generation and conversion, home appliances, automotive, and industry. He is the Principal Investigator of research contracts with industries, and also research projects funded by national and european Institutions. He is the author of more than 300 international publications on electric machines and drives (Scopus H-index 51). He has given seminars and invited presentations in international conferences and foreign universities. He is the Chairman of the IEEE IA/IE/PEL North Italy Joint Chapter, a Member of the Scientific Committee of national and international conferences and associations, reviewer of international scientific journals and evaluator of research projects in national and international programmes. He was the Head of the Department of Electrical Engineering from 2001 to 2008, a Member of the Scientific Committee of the University of Padova from 2004 to 2008, and the Vice-Rector for the Research from 2009 to 2015. His teaching activity at the University of Padova dealt with courses of Electromagnetic fields and Electrical circuit theory and, later, with Electric traction, Electric drives, Design of electric machines, Industrial electrical applications.

PAOLO GHERARDO CARLET (Member, IEEE) received the B.S. and M.S. (Hons.) degrees in 2015 and 2017, respectively, in electrical engineering from the University of Padova, Padova, Italy, where he is currently working toward the Ph.D. degree with Electrical Drives Laboratory, under the supervision of Prof. Silverio Bolognani. From August 2019 to June 2020, he was a Visiting Student with the Automatic Control Laboratory of ETH Zurich, Switzerland, under the supervision of Prof. Florian Dorfler. During the visiting period, he worked on the development of data-driven predictive control schemes for electric drives applications. His main research interests include data-driven control schemes and adaptive control algorithms, with particular focus on electric motor drives applications. The main tools he adopts to tackle these problems are model predictive control schemes, recursive state and parameters estimators and moving horizon estimation algorithms. The purpose of his research activity is to improve the performance of optimal control algorithms through the effective use of measured data.

FABIO TINAZZI (Member, IEEE) received the B.S., M.S., and Ph.D. degrees in mechatronic engineering from the University of Padova, Padova, Italy, in 2008, 2011, and 2015, respectively. Since January 2021, he has been a Researcher with the Department of Management and Engineering, University of Padova, Vicenza, Italy. His main research interests include sensorless control, predictive control, and parameter estimation techniques for ac motors.

MAURO ZIGLIOTTO (Senior Member, IEEE) is a native of Vicenza, Italy. He is currently a Full Professor of electrical machines and drives with the University of Padova, Padova, Italy, and the Head of Electric Drives Laboratory, Vicenza, Italy. His main research interests include advanced control strategies and self-commissioning for ac motors. He is the Secretary of the IEEE IAS-IESPELS North Italy Joint Chapter.